Clinkerless slag-silica binder: hydration process and hardening kinetics (part 2)

G.S Slavcheva[a]*, O.V. Artamonova[b], M.A. Shvedova[b], M.A. Khan[c]
a Voronezh State Technical University, Voronezh, Russia
b Voronezh State University of Architecture and Civil Engineering, Voronezh, Russia
c Karaganda State Technical University, Karaganda, Republic of Kazakhstan
* E–mail: gslavcheva@yandex.ru

Abstract. In part 1 of the studies, it was shown the results of the implementation of the "top–down" nanotechnological principle to obtain clinkerless binder with a high content of microsilica, activated during grinding what allowed to increase their hydraulic activity. Part 2 of the studies have been implemented in order to ensure the possibility of using of clinkerless slag-silica binder, modified by complex additive of SiO_2 nanoparticles in combination with a plasticizer ("bottom–up" nanotechnological principle), as a hydraulic binder. For nanotechnological activation the solution of nano-additives, synthesized by the sol–gel process, is used. Experimental results of changes phase composition and microstructure of clinkerless slag-silica binder during hydration and structuration processes; flocculation and hardening kinetics are presented. The laser granulometry method, dynamic light scattering and transmission electron microscopy were used to estimate the particle size of original components. XRD – method, scanning electron microscope were used to estimate phase composition and morphology of the clinkerless binder's hydration product. The flocculation was evaluated by the penetrometric method. The hardening kinetics was evaluated by the mechanical tests after 1, 3, 7, 14, 28 day of curing. As a result, the distinctive features of the main periods of heterogeneous processes of structure formation of the nano-activated clinkerless slag-silica binder are revealed at the different stages of hardening. It was established that the "bottom – up" nanotechnological principle, implemented through the introduction of SiO_2 – nanoparticles into binder paste allows to increase the hydraulic activity of slag due to the catalytic role of nanoparticles and their chemical interaction with slag minerals. As a result, the strength of the of clinkerless slag-silica binder was 35.8 MPa, and it's setting and hardening rates corresponds to the speed of these processes for Portland cement under normal temperature-humidity conditions.

1. Introduction

Currently, slag-alkaline binders represent a promising alternative to the cement [1–5]. Using industrial waste instead of expensive clinker in the production of slag-alkaline binders significantly reduces the final cost of the products and structures. An important moment when using binders of this type is the activation of the slag in their composition. The activation process is aimed at increasing the reactivity of the slag minerals and hydraulic activity of the binder which allows one to obtain products with high strength and durability [6, 7].

The following methods are known to increase the hydraulic activity of a binder [8]: mechanical grinding, mechanothermal activation of the slag component, the introduction of chemical additives, directional crystallization while lowering the basicity of the dispersed phase and complicating the composition.

The simplest, however, energy-consuming method of activating blast furnace slag is the fine grinding in the presence of activators. This method meets the nanotechnological principle of "top–down" [9]. The results of our research [10] confirmed the effectiveness of such activation of the clinkerless slag-silica binder at the manufacturing stage, as well as the use of the hydraulic potential of nano- and micro-sized particles at the hardening stage. Thus, it was found that the presence of a large amount of silica fume in the ultramicrodispersed state in the clinkerless slag-silica binder allows us to increase the hydraulic activity of the

binder and ensure its setting and hardening rate under normal temperature and humidity conditions, comparable to the speed of these processes for Portland cement.

It is known that for the modification of cement systems at present [11–17], not only micro- and ultrafine additives are widely used but also nano-additives that are introduced into cement paste. In a number of works it was established [18–20] that, with the introduction of nano-additives, similar effects are possible not only in cement but also in slag-alkaline clinkerless systems. So, in [18], it was shown that the introduction of 1.5–2 mass. % nano-clay into alkali and geopolymer mortars increases the strength of the resulting composites by 15–24 %, and the addition of nano-sized TiO2 particles reduces their shrinkage [19]. In [20], nanosilica was used to activate a slag-alkali binder. It was established that its introduction into the system under study contributes to the acceleration of the formation of gel-like hydrosilicates and calcium aluminosilicates, which leads to a quick set of the strength of the slag-alkaline paste. According to the scientific concept that authors formulated earlier [4], this approach to modification corresponds to the "bottom – up" nanotechnological principle. According to author's studies [18], the most effective for cement systems are complex additives (CND) based on SiO2 nanoparticles and superplasticizer (SP). SiO2 nanoparticles play a catalytic role, acting as crystallization centers, and also directly participate in the chemical interaction with cement clinker minerals during cement hydration. At the same time, our studies proved the possibility of accelerating the hydration processes of cement clinker by 20–25 times, as well as increasing the strength of cement composites by 1.5–2 times.

The effectiveness of CND application for cement systems that we established allows us to suggest that its use can also ensure the activation of slag and acceleration of the hydration and hardening processes of the clinkerless binder.

In part 1 of the studies [10] it was shown the results of the implementation of the "top–down" nano technological principle to obtain CSSB1 clinkerless binder, the characteristics of which comply with the physicomechanical characteristics of 32.5 cement according to EN 197-1:2000 "Cement – Part 1: Composition, specifications and conformity criteria for common cements". The research results presented in this article are an integral part and continuation of the work. The research results discussed in the article examine the possibility and evaluate the effectiveness of nano-technological activation of the slag-alkaline system according to the "bottom-up" principle in comparison with activation according to the "top – down" principle.

The work aimed to assess the possibility of using clinkerless slag-silica binder (CSSB2), modified with a complex nano-sized additive based on SiO2 (CND), as a hydraulic binder of normal hardening based on comprehensive studies of phase composition, structuration process, and hardening. The research objectives included:

– study of changes in phase composition and CSSB2 microstructure during hydration and structuration processes;

– comparative assessment of flocculation and hardening kinetics of two types of clinkerless binders CSSB1 and CSSB2;

– assessment of the effectiveness of using nanotechnological principles to activate clinkerless binders.

2. Methods[1]

The systems shown in Table 1 were investigated. The following raw materials were used to obtain clinkerless slag-silica binder:

– granulated blast-furnace slag from LLP "Arcelor Mittal" plant (Temirtau, Kazakhstan) with a lime factor of 0.75;

– microsilica of MKU-95 grade with a mass fraction of SiO_2 = 96.85 %;

– building lime of an activity of 86.2 %;

– gypsum (gypsum dehydrate);

– powder superplasticizer S-3 based on naphthalenesulfonates,

– superplasticizer of Sika trademark based on polycarboxylic ethers (SP).

---

[1] The studies were conducted in the laboratory of the Center for Collective Use named after Professor Yu.M. Borisov (Voronezh State Technical University, Russia)

Slavcheva, G.S., Artamonova, O.V., Shvedova, M.A., Khan, M.A.

Table 1. Mixture composition.

Systems	Specimen ID	W/C, W/CSSB	Components		Dosage, %	Specific surface area S_u, m²/kg
cement +CND	C + CND	0.33	cement CEM I 42.5N		99.79	300
			CND	NP SiO₂	0.01	1.42·10⁶
				SP	0.2	
clinkerless slag-silica binder +water	CSSB1 + W	0.30	granulated blast-furnace slag		63	900
			microsilica		20	
			building lime		14	
			gypsum		1.5	
			S-3		1.5	
clinkerless slag-silica binder + CND	CSSB2 + CND	0.20	granulated blast-furnace slag		63	740
			microsilica		14	
			building lime		1.5	
			gypsum	NP SiO₂	0.01	1.42·10⁶
				SP	0.2	

For nanotechnological activation of CSSB2, CND solution was used, a detailed sol – gel synthesis of which was described in [17]. The manufacturing conditions and characteristics of CSSB1 are presented in [10]. The CND modified cement system with a SiO₂ nanoparticles dosage of 0.01 % (NP), what was previously studied in detail [18], was taken as a reference.

In preliminary exploratory studies, CND with a dosage of SiO₂ nanoparticles of 0.01 %, 0.05 %, and 0.1 % by weight of the binder was used for nano-modification of the cinder-alkali binder. It was found that slag-alkali systems with nanoparticle dosages of 0.05 % and 0.1 % underwent self-destruction during the removal of samples. Thus, for a clinkerless binder, as well as for cement systems [17], the optimal SiO₂ nanoparticles dosage is 0.01 % by weight of the binder. Therefore, all studies for CSSB2 + CND were conducted with this dosage.

The amount and size of the colloidal nanoparticles SiO₂ synthesized by the sol – gel process were determined using dynamic light scattering (Photocor Complex spectrometer), and transmission electron microscopy (TEM) (Transmission Electron Microscope H-9500, v_{acs} = 75 kV).

Operational control of the binder dispersion by its specific surface area was carried out by the method of air permeation on the PSH-8A device. The particle sizes of the microsilica and binder were studied using the laser particle size analyzer ANALYSETTE 22 Nano Tec.

The structuration process, flocculation, and hardening kinetics were studied in the C+CND, CSSB1+W and CSSB2+CND systems. W/C – ratio and W/CSSB – ratio of these systems were different, what were assigned based on the standard normal consistency of fresh pastes.

The phase composition of the clinkerless binder was controlled by the XRD-method (ARL X'TRA diffractometer, CuKα radiation (λ = 1.541788 Å) after 1, 3, 7, 14, 28 days of hardening under normal temperature and humidity conditions. X-ray decoding and phase identification were carried out using PDWin 4.0 [21].

The morphology of the hardened cement and CSSB paste structure was examined on a JEOL JSM-7001F scanning electron microscope.

After mixing the CSSB with water, the flocculation process of fresh binder paste was controlled in two ways. The setting times were determined on a Vicat-method according to Russian State Standard GOST 30744-2001 "Cements. Methods of testing with using polyfraction standard sand".

The flocculation (setting kinetics) of fresh binder paste was evaluated by the plastic strength index $P_{pl.}$ determined using a universal penetrometer Geopocket S068. To determine the plastic strength, fresh binder paste was placed in a ring with a diameter of 150 mm and a height of 55 mm. The determination of plastic strength was performed by immersing a standard penetrometer plunger (6.4 mm) to a predetermined mark (to a depth of 5 mm). The readings were taken on an internal scale in kgf/cm², the value of plastic strength P_{pl} was determined based on the fact that 1 kgf/cm² = 98.0665 kPa. Tests were carried out from the moment the mixture was prepared until the moment it began to set (determined using a Vicat-method) every 15 minutes. For each test period, 12 measurements were made.

The CSSB hardening kinetics was evaluated by testing samples – cubes 5×5×5 cm in size after 1, 3, 7, 14, 28 days of curing under normal temperature and humidity conditions (t = 20 °C, RH = 95 ± 5 %). The strength testing was carried out on a universal 4-column floor hydraulic test system INSTRON Sates 1500 HDS. As a result of the tests, the full diagrams "strain σ – displacement Δ" were obtained. According to the tests, the compressive strength and elastic modulus were determined. To ensure the statistical reliability of the results of physical and mechanical tests, the number of samples in the series was 6 pieces. The intra-series coefficient of variability of the test results was 5–7 %.

3. Results and Discussion

The specific surface area of binders in the CSSB1 + W and CSSB2 + CND systems is S_u = 900 and S_u = 740 m²/kg, respectively. CSSB2 was ground to a lesser degree of dispersion since its activation is carried out by introducing CND.

According to the methods of transmission microscopy (Fig. 1 a) and dynamic light scattering (Fig. 1 b), (Table 2) the average particle size of SiO_2 is approximately 5–10 nm. Moreover, the CND complex additive based on them is stable for seven days from the moment of synthesis [8]. Microsilica as part of a slag-alkaline binder is an almost mono-dispersed system [5] with an average particle diameter of 15.6 µm.
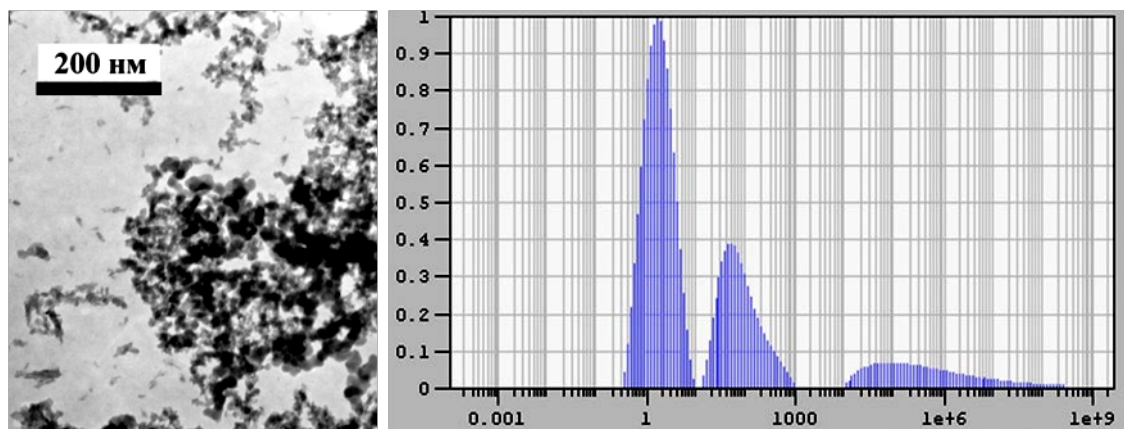
**Figure 1. Size and range of SiO2 - nanoparticles as part of CND
after 7 days from the moment of synthesis:
a) micrographs (TEM data); b) particles range (hydrodynamic radius is presented).**

Table 2. Sizes of nano- and microparticles.

Name	Data (Analyzette22, PhotocorComplex)	
	ω particles, %	d, µm
Nanosilica	28	0.002
	39.3	0.005
	27.3	0.01
Microsilica	93	15.6
	7	≤15.6

In [10], it was shown that the slag we used to obtain clinkerless slag-silica binders is in an amorphized state. In this case, the mellitic phase ($8CaO \cdot 3Al_2O_3 \cdot MgO \cdot 5SiO_2$) is registered, which in the presence of activators can exhibit binding properties.

The CSSB2+CND system (Fig. 2) is dominated by the phases of highly basic calcium hydrosilicate ($2CaO \cdot SiO_2 \cdot H_2O$) and calcium hydroaluminosilicate ($CaO \cdot Al_2O_3 \cdot 2SiO_2 \cdot 4H_2O$), which are present in the system throughout the entire hardening time. Also, a small number of tobermorite-like phases ($xCaO \cdot SiO_2 \cdot zH_2O$, $(CaO)_x \cdot SiO_2 \cdot zH_2O$) are detected in this system, which appear in the system on the first day of hardening and their number gradually increases over time. In addition, on the first day of hardening, a small amount of the portlandite phase ($Ca(OH)_2$) is registered in the system, and then the amount of this phase decreases.

X-ray analysis of samples at the age of 28 days of hardening shows that all three systems differ in phase composition (Fig. 3).

In the C+CND system, tobermorite-like phases of the composition $xCaO \cdot SiO_2 \cdot zH_2O$, $(CaO)_x \cdot SiO_2 \cdot zH_2O$, as well as the phase of low-basic calcium hydrosilicate $CaO \cdot SiO_2 \cdot H_2O$ are recorded. The amount of these phases increases over time. The phases of ettringite and portlandite are absent in this system [10]. The

CSSB1+W system is characterized by the presence of tobermorite-like phases and highly basic calcium hydrosilicates ($6CaO \cdot 4SiO_2 \cdot 3H_2O$). Also, there is a small number of phases of calcium hydroaluminosilicate with the composition $CaO \cdot Al_2O_3 \cdot 2SiO_2 \cdot 2H_2O$, ettringite ($3CaO \cdot Al_2O_3 \cdot 3CaSO_4 \cdot 31H_2O$) and portlandite in this system. In contrast to the above systems, the largest amount of the phase of calcium hydroaluminosilicate ($CaO \cdot Al_2O_3 \cdot 2SiO_2 \cdot 4H_2O$) is observed for CSSB2 + CND, and small amounts of tobermorite, low-basic calcium hydrosilicates, ettringite are also recorded.

1. It should be noted that in all the samples, diffraction peaks are mixed, which is associated with the multicomponent nature of the systems and the possible formation of crystalline phases of an ultra-dispersed and nano-size scale. The obtained X-ray diffractometric data correlate well with the results of scanning electron microscopy (SEM).

2. According to SEM, the microstructure of the studied systems is also significantly different (Fig. 4). At the microscale level (Fig. 4 a, b) both systems are microheterogeneous with inclusions of pores of various sizes. However, in the CSSB1 + W system, there are more capillary pores (Fig. 4 a), which is naturally associated with a larger W/C value for this system.

3. As it increases, it is observed (Fig. 4 c, d) that the CSSB1+W system has a denser and more uniform structure. At the same time, the structure CSSB2+CND contains inclusions of relatively large slag grains that are not registered in the structure CSSB1+W. This is due to the greater dispersion of CSSB1 ($S_{u.} = 900$ m²/kg in comparison with $S_{u.} = 740$ m²/kg for CSSB2) and the presence in CSSB1 of a significant amount of microsilica, which provides denser packing of hydration products.

4. The microstructure of hydration products for both systems is mainly represented by lamellar morphology crystallites characteristic of the phases of low-basic calcium hydrosilicates (Fig. 4 e, f, g, h). Particles of hydration products are of various sizes and have a large number of contacts of abutment, coalescence, and intergrowth. Moreover, large needle crystals are observed in the CSSB1+W system, which, according to the X-Ray method data, can be attributed to the ettringite phase (Fig. 4 e, g). A distinctive feature of the CSSB2+CND structure is the presence of large lamellar-prismatic crystals characteristic of calcium hydroaluminosilicate (Fig. 4 f, h).

According to the standard determination of the setting time, the beginning of setting CSSB2+CND is registered after 80 minutes of exposure at a value of $P_{pl} = 412$ kPa. In this case, the setting kinetics of the CSSB2+CND system is characterized (Fig. 5) by an intensive increase in plastic strength over the entire flocculation period, in contrast to the CSSB1+W system. For CSSB1+W, an increase in plastic strength is practically not observed for 80 min, the onset of setting was recorded after 150 minutes at $P_{pl} = 387$ kPa.

It is established that the form of strain diagrams for the studied systems differs non-substantially. For hardened paste CSSB2+CND (Fig. 6), as well as for CSSB1+W [10], at the age of 1 day, the elasticity area is absent on the diagram and the destruction occurs according to the pseudoplastic type. On the deformation diagrams of CSSB2+CND samples that hardened for 3, 7, 28 days, the elastic area is clearly registered, the length of the descending branch of the diagram is reduced. Thus, as hardening increases, the rigidity increases and the ductility of the system decreases. In both hardened CSSB-pastes at the age of 14 days, a reappearance of the area of plastic deformations was recorded, which corresponds to a temporary decrease in the elastic modulus (Table 3). Despite the similar nature of the destruction, the hardened paste CSSB2+CND is more fragile. With almost the same strength, the elastic modulus values of CSSB2+CND are 1.5–3 times higher than for CSSB1 + W.

Table 3. Hardening kinetics data.

Time, days	1	3	7	14	28
C + CND					
Compressive strength, MPa	64.1	73.0	69.8	83.1	92.7
CSSB1 + W					
Compressive strength, MPa	4.7	14.6	17.1	21.0	37.5
Young's modulus, MPa	340	1390	1536	776	3398
CSSB2 + CND					
Compressive strength, MPa	2.6	12.6	31.9	22.6	35.8
Young's modulus, MPa	177	1690	4112	852	4113

According to the kinetic hardening curve (Fig. 7), the strength increase of CSSB2+CND in the period up to 7 days of hardening is more intense than for CSSB1+W. In the period of 1–7 days, the strength of CSSB2+CND increases 12 times, the strength of CSSB1+W – 4 times. However, for CSSB2+CND, a sharp drop in strength on the 14th day of hardening was recorded. As a result, the strength achieved by the 28th day by both systems has comparable values. Of course, the growth rate and the achieved strength values for

hardened CSSB pastes are significantly lower than for the standard hardened cement paste C+CND. Nanomodification of the cement system allows one to provide 28-day strength normalized for CEM 42.5N already by 1 day of hardening, and the final strength of this system reaches almost 100 MPa. However, the hardening kinetics data results for CSSB pastes suggest that both nanotechnological activation techniques used provide efficient hardening of clinkerless binders without heat treatment, under normal temperature and humidity conditions (t = 20 ºC, RH = 95 ± 5%).
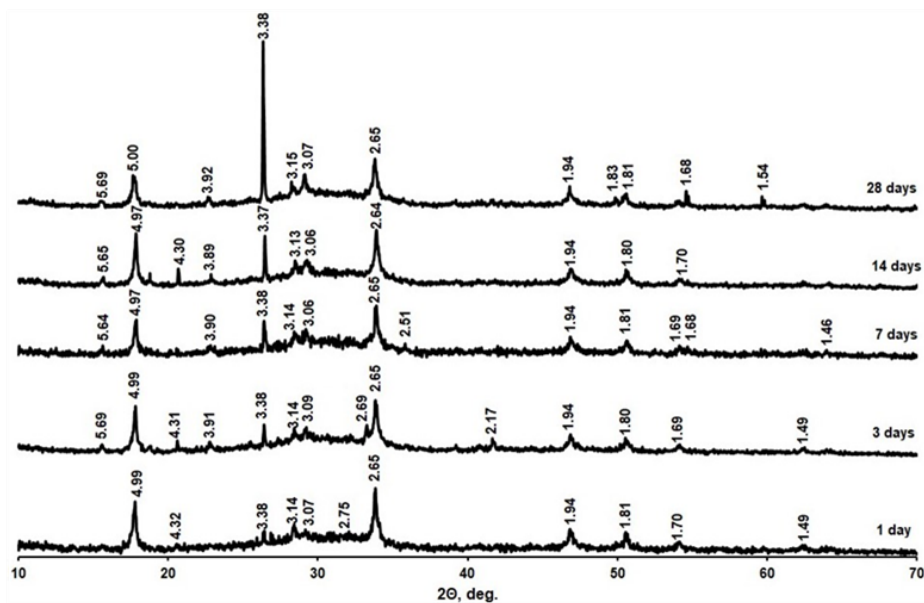
Figure 2. X-Ray Diffraction pattern of hardened paste CSSB2 + CND.
Designations:
2CaO·SiO2·H2O (d = 3.34, 2.92, 2.25, 1.86, 1.75);
CaO·Al2O3·2SiO2·4H2O (4.96, 3.24, 3.14, 2.67, 1.78,
xCaO·SiO2·zH2O (d = 3.07, 2.65, 1.83, 1.67, 1.53);
(CaO)x·SiO2·zH2O (d = 4.92, 3.34, 3.05, 1.83, 1.67);
Ca(OH)2 (d = 4.93, 3.11, 2.63, 1.93, 1.79)
**3CaO·Al2O3·3CaSO4·31H2O (d = 4.98, 3.88, 1.90, 1.87, 1.76)**
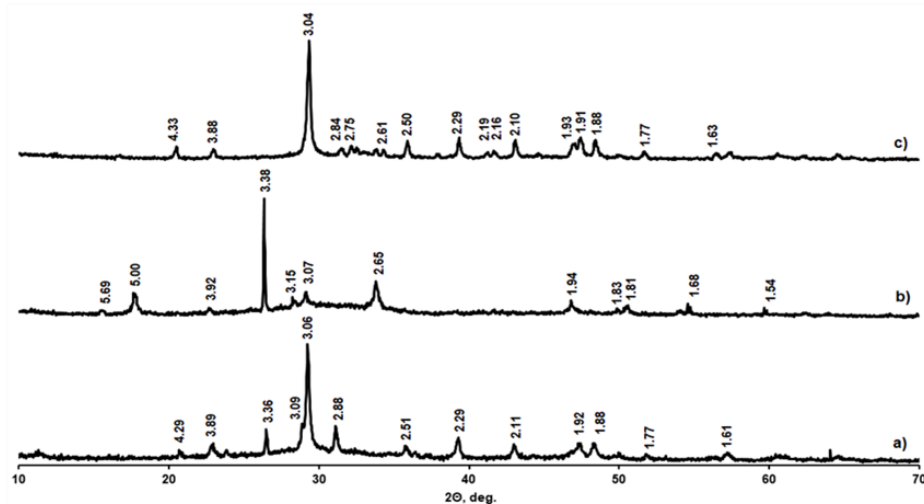
Figure 3. X-Ray Diffraction pattern of hardened system (28 days of hardening):
a) CSSB1 + W, b) CSSB2 + CND, c) C + CND.
Designations:
6CaO·4SiO$_2$·3H$_2$O (d = 4.31, 3.11, 2.26, 1.95, 1.76);
2CaO·SiO$_2$·H$_2$O (d = 3.34, 2.92, 2.25, 1.86, 1.75);
CaO·SiO$_2$·H$_2$O (d = 3.21, 3.01, 2.78, 2.23, 2.01, 1.77);
(CaO)$_x$·SiO$_2$·zH$_2$O (d = 4.92, 3.05, 2.93, 2.80, 1.83);
xCaO·SiO$_2$·zH$_2$O (d = 3.07, 2.97, 2.80, 2.28, 1.83);
CaO·Al$_2$O$_3$·2SiO$_2$·4H$_2$O (d = 4.91, 4.27, 3.34, 3.19, 2.70);
3CaO·Al$_2$O$_3$·3CaSO$_4$·31H$_2$O (d = 4.98, 3.88, 1.90, 1.87, 1.76)
Ca(OH)$_2$ (d = 4.93, 3.11, 2.63, 1.93, 1.79)
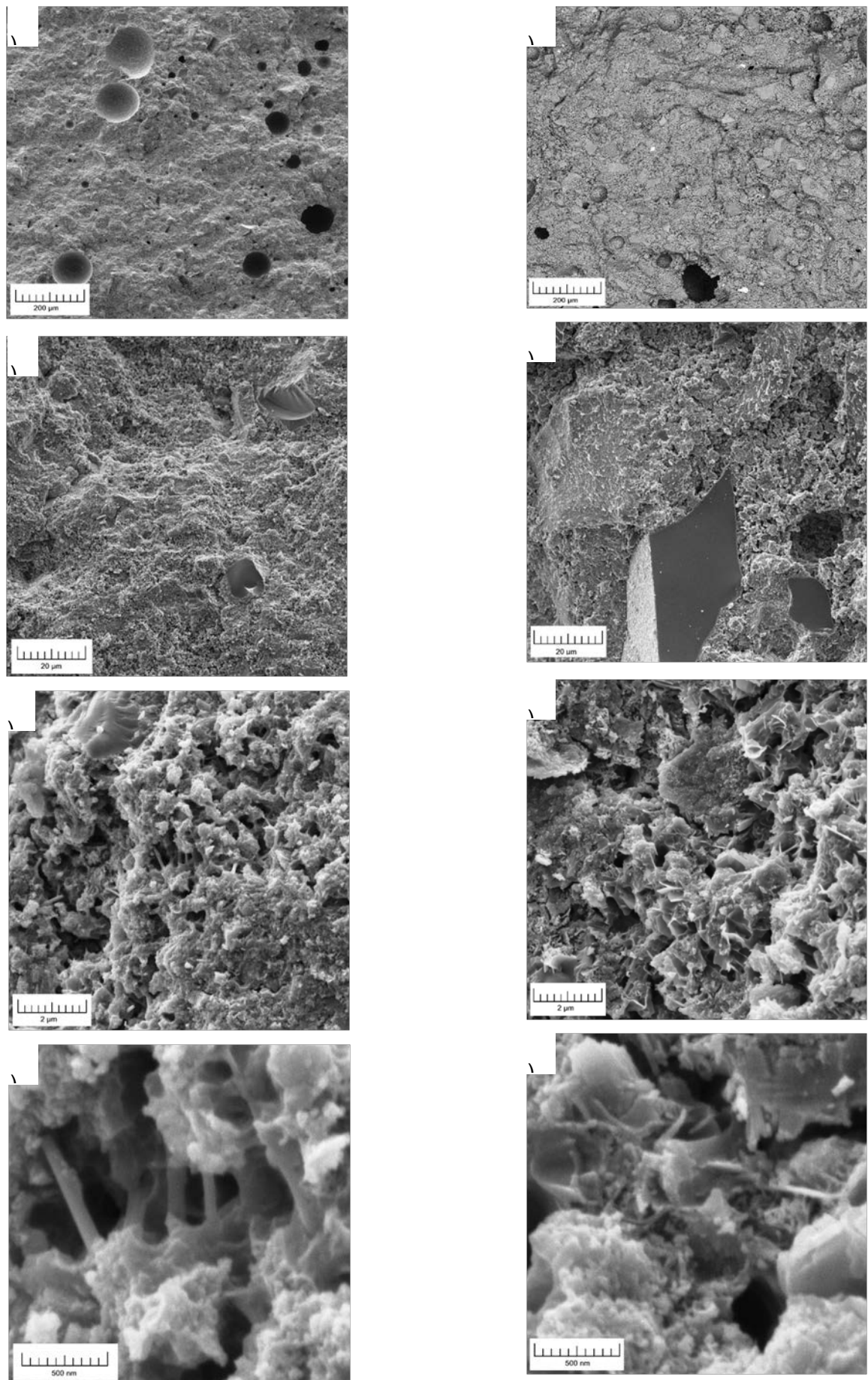
Figure 4. SEM images of hardened CSSB-pastes:
**a, c, e, g) CSSB1 + W; b, d, f, h) CSSB2 + CND.**
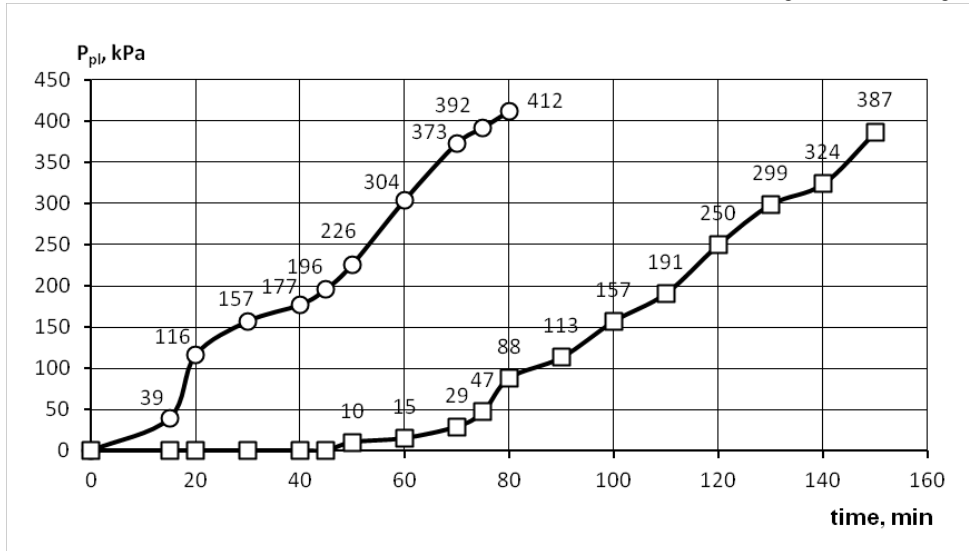
Figure 5. Flocculation kinetics of fresh CSSB-pastes
Designations: □ – CSSB1 + W; ○ – CSSB2 + CND.
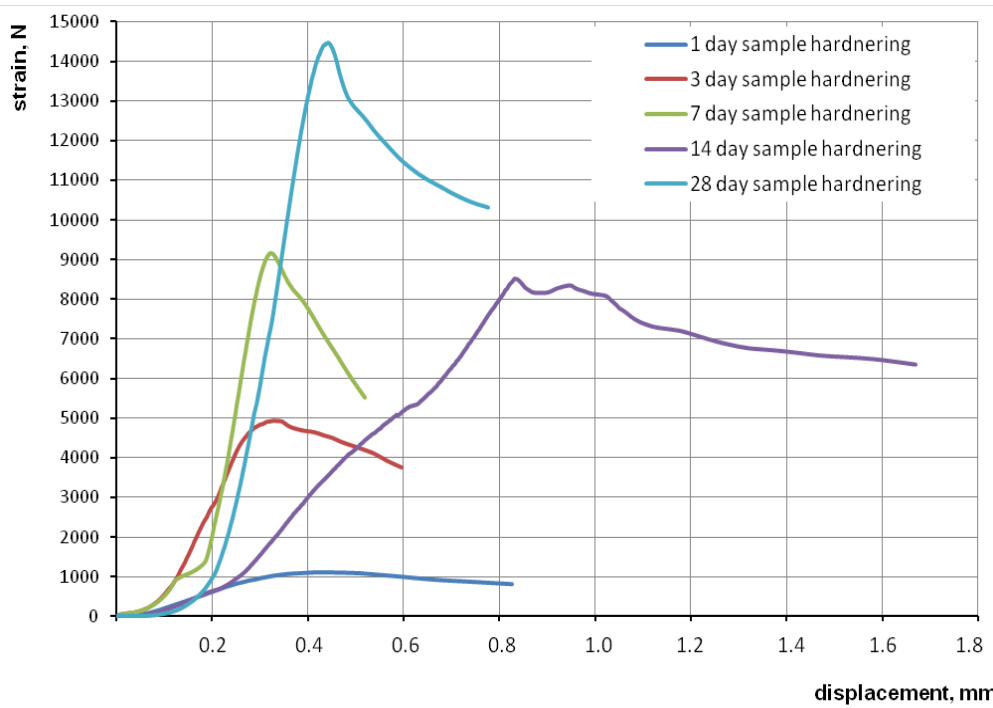

Figure 6. Tested hardened CSSB2 pastes "strain s - displacement Δ" experimental results.
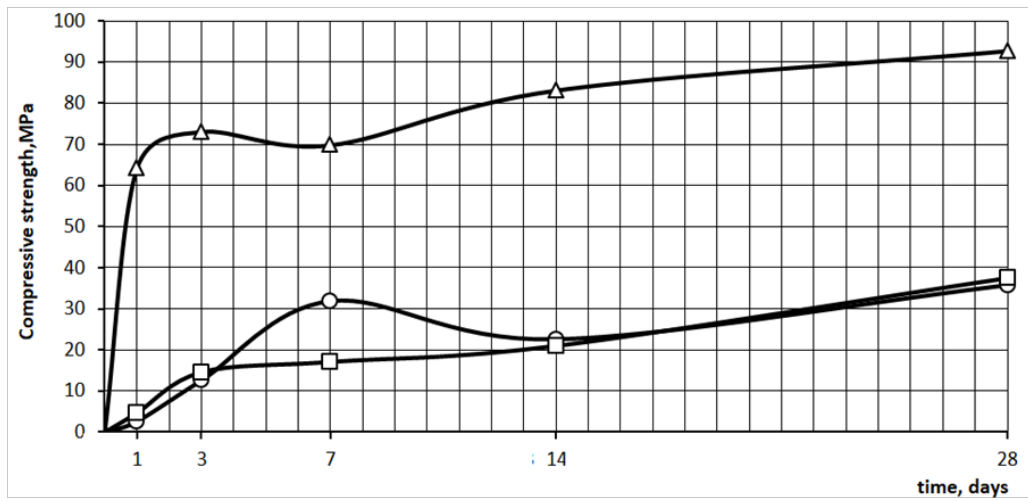

Figure 7. Hardening kinetics of CSSB-pastes and cement paste
Designations: □ – CSSB1 + W; ○ – CSSB2 + CND; Δ - C + CND.

In [10], it was shown the differences in hydration and hardening of the clinkerless slag-silica binder CSSB1 compared to the traditionally distinguished periods of the hydration of cement systems, namely, the *initial* and *pre-induction, induction*, acceleration, deceleration and slow interaction. In the framework of this approach, let us compare the features of hydration processes for all the studied nano-modified systems.

According to the flocculation curve (see Fig. 5) for CSSB1, the set of plastic strength begins after 80 min exposure, which is due to the slow dissolution of the slag grains and the delay in the onset of hydration phases. On the contrary, CSSB2 is characterized by an intensive increase in plastic strength almost from the moment of mixing. This can be attributed to the catalytic role of SiO_2 nanoparticles, which intensify the processes of hydration phase nucleation. As a result, the setting start time for CSSB1 (150 min) corresponds to the standard setting start time range for Portland cement (120-160 min), and for CSSB2 the setting start time is faster (80 min).

For the C + CND nanomodified system, the acceleration period is associated with the formation of a spatial framework in the system as a result of mass crystallization of low-basic tobermorite-like hydrosilicates [4], which determines its high strength already on the 1st day of hardening. On the contrary, for both types of CSSB at this period, highly basic primary calcium hydrosilicates $2CaO \cdot SiO_2 \cdot H_2O$ prevail in the hydration products. They belong to the dendrid-like and amorphous morphological type, which have low strength of crystallization contacts [22]. Therefore, it is logical that, by the first day of hardening, the CSSB1 + W and CSSB2 + CND systems have an abnormal deformation diagram for solids (see Fig. 6), low strength and elastic modulus.

In the period of 1–7 days of hardening for CSSB2 + CND, a more intensive increase in the strength of the system and its elasticity occurs than for CSSB1 + W. The elastic area is clearly defined on the deformation diagrams of both systems, which may be due to the formation of a crystalline framework in hydration products (secondary phases of $6CaO \cdot 4SiO_2 \cdot 3H_2O$ hydrates of fibrous-needle morphology, ettringite crystals, and AFt-phases). A more intensive increase in the strength of CSSB2 + CND may be due to the formation of tobermorite-like phases in it, as they provide the greatest number and strength of contacts per unit volume. In the hydration products of CSSB1 + W, tobermorite-like phases are not registered at this time [10]. The presence of secondary hydrates, a rapid increase in strength allows us to correlate the period of 1 to 7 days with the period of slowdown of the hydration process for both clinkerless systems.

In comparison with clinkerless systems, it is necessary to emphasize that due to nanomodification, the C + CND cement system reaches 70 % of its maximum strength by the 3d day of hardening, the entire subsequent period of its hardening (3–28 days) refers to the stage of slow interaction.

However, further, characteristics of the hardening process of CSSB1 + W and CSSB2 + CND are significantly different. In the period of 3–14 days for CSSB1 + W there is only a slowdown in the set of strength, and for CSSB2 + CND – a decrease in strength by 1.5 times from the value reached by the 7th day.

The strain diagram for both systems on the 14th day of hardening again acquires an anomalous character, characterized by a long plateau of pseudoplastic deformations. This is naturally accompanied by a decrease in the elastic modulus for CSSB1 + W by half, for CSSB2 + CND – by 4 times in relation to its value at the age of 7 days. The change in the elastic-plastic behavior can be associated with the repeated mass formation of primary hydrates $2CaO \cdot SiO_2 \cdot H_2O$, which is especially significant for CSSB2 + CND due to the chemical interaction of SiO_2 nanoparticles with the slag minerals. As a result, the crystallization pressure in the already formed crystalline framework determines a significant decrease in strength.

In the period of 14–28 days, there is an increase in the strength and elasticity of CSSB1 + W and CSSB2 + CND, which can be correlated with the *processes of self-organized structure formation*. In the hardening system CSSB2 + CND, the content of low-basic calcium hydrosilicates, which are represented by crystallites of lamellar morphology, increases (Fig. 4 f, h). CSSB1 + W is characterized by the presence of well-formed ettringite crystals in the structure (Fig. 4 e, g), which provide an increase in the energy of destruction due to microreinforcement of the structure.

It is important to emphasize that during all the hardening periods, the Portlandite $Ca(OH)_2$ phase is practically absent in the composition of the CSSB1 and CSSB2 hydration products. This indicates that the solution very quickly reaches saturation with $HSiO_3^-$, SiO_3^{2-}, $H_2SiO_4^{2-}$, Al^{3+}, AlO_2^- ions, which bind Ca^{2+}, $CaOH^+$ cations to hydrated compounds, preventing the crystallization of Portlandite $Ca(OH)_2$. Also, as part of hydration products of CSSB1 and CSSB2, one of the least active slag phases, the mellitic phase $8CaO \cdot 3Al_2O_3 \cdot MgO \cdot 5SiO_2$, almost immediately ceases to be registered. On this basis, it can be argued that both obtained binders are characterized by high hydraulic activity. For CSSB1, this is ensured by the good solubility of ultramicrodispersed particles with a diameter of $d \sim 1–6$ µm with an amorphized surface. This is the result of mechanochemical activation of CSSB1 during grinding in the presence of S-3 superplasticizer as a complex of surfactants. For CSSB2, hydraulic activity is largely determined by the catalytic role of SiO_2 nanoparticles at the acceleration stage, and their chemical interaction with the slag minerals at the stages of deceleration and slow interaction during hydration.

Slavcheva, G.S., Artamonova, O.V., Shvedova, M.A., Khan, M.A.

4. Conclusions

1. The phase composition of hydration products of clinkerless slag-silica binder CSSB2, activated by a complex additive based on SiO_2 nanoparticles, is characterized by the presence of tobermorite phases, low-basic calcium hydrosilicates, ettringite, and a significant content of AFt-phases. At the micro-scale level, the structure of the hardened binder paste is microheterogeneous with inclusions of pores of various sizes and grains of slag. The microstructure of hydration products is mainly represented by lamellar morphology crystallites, which are of different sizes and have a large number of contacts of abutment, coalescence, and intergrowth.

2. The clinkerless binder CSSB1 obtained by mechanochemical activation is characterized by the onset of setting in 150 minutes, a strength of 17.1 MPa at the age of 7 days, 37.5 MPa at 28 days. The clinkerless binder CSSB2, activated by a complex additive based on SiO_2 nanoparticles, is characterized by the onset of setting in 80 minutes, a strength of 31.9 MPa at the age of 7 days, 35.8 MPa at 28 days. The setting and strength indicators of the resulting clinkerless slag-silica binder types meet the physicomechanical characteristics of cement grade 32.5 EN 197-1:2000 "Cement – Part 1: Composition, specifications and conformity criteria for common cements".

3. The results of a comprehensive assessment of the characteristics of the two types of clinkerless slag-silica binders and the parameters of their structure formation and hardening made it possible to confirm the effectiveness of using nano technological "bottom – up" principles to activate the hydration and hardening processes. The "top – down" principle, realized through mechanochemical activation of the binder components during grinding, allows one to provide almost 50% content of ultramicrodispersed particles with a diameter of d ~ 1–6 μm and increase their hydraulic potential. The "bottom – up" principle, implemented through the introduction of SiO_2 nanoparticles into binder paste, allows increasing the hydraulic activity of slag due to the catalytic role of nanoparticles and their chemical interaction with the slag minerals. This made it possible to provide a setting and hardening rate for the obtained clinkerless binders under normal temperature and humidity conditions (t = 20 ºC, RH = 95 ± 5%), comparable with the speed of these processes for Portland cement.

4. The development of research involves the study of the possibilities of producing concrete based on the developed types of clinkerless binders for the production of building products and structures both in factory and in building conditions.

5. Acknowledgement

References

1. Sun, J., Zhang, Z., Zhuang, S., et al. Hydration properties and microstructure characteristics of alkali–activated steel slag. Construction and Building Materials. 2020. V. 241. Pp. 118141. DOI: https://doi.org/10.1016/j.conbuildmat.2020.118141

2. Karim, M.R., Hossain, M.M., A Elahi, M.M., et al. Effects of source materials, fineness and curing methods on the strength development of alkali-activated binder. Journal of Building Engineering. 2020. V. 29. Pp. 101147. DOI: https://doi.org/10.1016/j.jo-be.2019.101147

3. Rostami, M., Behfarnia, K. The effect of silica fume on durability of alkali activated slag concrete. Construction and Building Materials. 2017. V. 134. Pp. 262–268. DOI: https://doi.org/10.1016/j.conbuildmat.2016.12.072

4. Ramezanianpour, A.A., Moeini, M.A. Mechanical and durability properties of alkali activated slag coating mortars containing nanosilica and silica fume. Construction and Building Materials. 2018. V. 163. Pp. 611–621. DOI: https://doi.org/10.1016/j.con-buildmat.2017.12.062.

5. Rakhimova, N.R., Rakhimov, R.Z. A review on alkali-activated slag cements incorporated with supplementary materials. Journal of sustainable Cement-Based Materials. 2014. V. 3 (1). P. 61. DOI: 10.1080/21650373.2013.876944

6. Rakhimova, N.R., Rakhimov, R.Z. Ompozicionnye shlakoshchelochnye vyazhushchie s kremnezemistymi mineral'nymi dobavkami [Composite slag-alkaline binders with silica mineral additives]. Inorganic materials. 2012. 9 (48). P. 1083. (rus)

7. Rakhimova, N.R., Rakhiov, R.Z. Alkali-activated cements and mortar based on blast furnace slag and redclay brick waste. Materials and design. 2015. 8. Pp. 324–331. DOI: 10.1016/j.matdes.2015.06.182

8. Bazhenov, Y.M., Zagorodnjuk, L.H., Lesovik, V.S., Yerofeyeva, I.V., Chernysheva, N.V., Sumskoy, D.A. Concerning the role of mineral additives in composite binder content. International Journal of Pharmacy and Technology. 2016. 8 (4). Pp. 22649–22661.

9. Lesovik, V.S., Alfimova, N.I., Trunov, P.V. Reduction of energy consumption in manufacturing the fine ground cement. Research Journal of Applied Sciences. 2014. 9 (11). Pp. 745–748. DOI: 10.3923/rjasci.2014.745.748

10. Slavcheva, G.S., Baidzhanov, D.O., Khan, M.A., et al. Clinkerless slag-silica binder: hydration process and hardening kinetics. Magazine of Civil Engineering. 2019. 92 (8). Pp. 96–105. DOI: 10.18720/MCE.92.8

11. Singh, N.B., Meenu, K., Saxena, S.K. Nanoscience of Cement and Concrete. Materials Today: Proceedings. 2017. 4 (4). Pp. 5478–5487. DOI: 10.1016/j.matpr.2017.06.003

12. Reches, Y. Nanoparticles as concrete additives: Review and perspectives. Constructions and Building Materials. 2018. 175. Pp. 483–495. DOI: https://doi.org/10.1016/j.conbuildmat.2018.04.214

13. Rai, S., Tiwari, S. Nano Silica in Cement Hydration. Materials Today: Proceedings. 2018. 5(3). Pp. 9196–9202. DOI: https://doi.org/10.1016/j.matpr.2017.10.044

Slavcheva, G.S., Artamonova, O.V., Shvedova, M.A., Khan, M.A.

14. Du, H., Pang, D. High performance cement composites with colloidal nano-silica. Construction and Building Materials. 2019. 224. Pp. 317–325. DOI: https://doi.org/10.1016/j.conbuildmat.2019.07.045

15. Kong, D., Pan, H., Wang, L., et al. Effect and mechanism of colloidal silica sol on properties and microstructure of the hardened cement-based materials as compared to nano-silica powder with agglomerates in micron-scale. Cement and Concrete Composites. 2019. 98. Pp. 137–149. DOI: https://doi.org/10.1016/j.cemconcomp.2019.02.015

16. Meng, T., Hong, Y., Wei, H. et al. Effect of nano-SiO2 with different particle size on the hydration kinetics of cement. Thermochimica Acta. 2019. 675. Pp. 127–133. DOI: https://doi.org/10.1016/j.tca.2019.03.013

17. Artamonova O.V., Slavcheva G.S., Chernyshov E.M. Effectiveness of combined nanoadditives for cement systems. Inorganic materials. 2017. 53 (10). Pp. 1080–1085. DOI: 10.1134/s0020168517100028

18. Assaedi, H., Shaikh, F.U.A., Low, I.M. Effect of nano-clay on mechanical and thermal properties of geopolymer. Journal of Asian Ceramic Societies. 2016. 4. Pp. 19–28. DOI: https://doi.org/10.1016/j.jascer.2015.10.004

19. Yang, L.Y., Jia, Z.J., Zhang, Y.M., et al. Effects of nano-TiO$_2$ on strength, shrinkage and microstructure of alkali activated slag pastes. Cement and Concrete Composites. 2015. 57. Pp. 1–7. DOI: 10.1016/j.cemconcomp.2014.11.009

20. Wang, J., Du, P., Zhou, Z., et al. Effect of nano-silica on hydratation, microstructure of alkali-activated slag. Construction and Building Materials. 2019. 220. Pp. 110–118. DOI: https://doi.org/10.1016/j.conbuildmat.2019.05.158

21. JCPDS – International Centre for Diffraction Data. © 1987–1995. JCPDS – ICDD. Newtown Square, PA. 19073. USA.

22. Artamonova, O.V., Slavcheva, G.S. Structure of cement systems as objects of nanomodification // Scientific Herald of the Voronezh State University of Architecture and Civil Engineering. Construction and Architecture. 2016. No. 1 (29). Pp. 13–26.

Contacts:

Galina Slavcheva, gslavcheva@yandex.ru

Olga Artamonova, ol_artam@rambler.ru

Maria Shvedova, marishwedowa@mail.ru

Maxim Khan, han_maks@mail.ru